Enhanced Photocatalytic Degradation of VOCs Using Ln^{3+}-TiO_2 Catalysts for Indoor Air Purification

F. B. Li[1,2], X. Z. Li[1*], C. H. Ao[1], S. C. Lee[1] and M. F. Hou[2]

[1]Department of Civil and Structural Engineering, The Hong Kong Polytechnic University, Hong Kong, China

[2]Guangdong Key Laboratory of Agricultural Environment Pollution Integrated Control, Guangdong Institute of Eco-Environmental and Soil Sciences, Guangzhou, 510650, China

Abstract: Two types of lanthanide ion-doped titanium dioxide (Ln^{3+}-TiO_2) catalysts including La^{3+}-TiO_2 and Nd^{3+}-TiO_2 were prepared by a sol-gel method. The effects of the lanthanide ion doping on the crystal structure, surface area, adsorption properties, pore size distribution, and surface chemical state of the catalysts were investigated by means of XRD, BET, and XPS. As results, the crystal size decreased significantly, while the specific surface area, t-plot total surface area, micropore volume, and the total pore volume increased owing to the lanthanide ion doping. The nitrogen adsorption-desorption isotherms of the catalysts showed that the N_2 adsorption ability of the Ln^{3+}-TiO_2 catalysts was better than the TiO_2 catalyst. Among them, the 0.7% Ln^{3+}-TiO_2 catalysts demonstrated the highest adsorption ability. The photocatalytic activity of the catalysts was investigated in the experiments of the photocatalytic degrdation of benzene, toluene, ethylbenzene and o-xylene (BTEX) in a gaseous phase. The photocatalytic efficiency of the TiO_2 catalysts with the lanthanide ion doping was remarkably enhanced by BTEX removal. The 1.2% Ln^{3+}-TiO_2 catalysts achieved the highest photocatalytic activity. The enhanced photodegrdation of BTEX is possibly due to the improved adsorption ability and the enhanced electron-hole pairs separation due to the presence of Ti^{3+} on the surface of Ln^{3+}-TiO_2 catalysts and the electron transfer between the conduction band/defect level and lanthanide crystal field state.

Keywords: BTEX; Indoor air purification; Lanthanide ion; Photocatalysis; TiO_2

---
* *Corresponding author: phone: (852) 2766 6016; Fax: (852) 2334 6389; Email: cexzli@polyu.edu.hk (X. Z. Li)*

1. Introduction

Indoor air quality (IAQ) within buildings is a critical concern, since many metropolitan generally spend more than 80% of time in an indoor environment. Recently the sick building syndrome has been paid great attention especially in some urban cities such Hong Kong and other major cities in China (Roberts and Nelson, 1995; Guo et al., 2003). Indoor air pollutants mainly include nitrogen oxides (NO_x) and volatile organic compounds (VOCs), which can cause adverse health impacts on occupants (Jones, 1999). VOCs are primarily composed of BTEX (benzene, toluene, ethylbenzene, and *o-x*ylene) and halogenated hydrocarbons (Maroni et al., 1995). These indoor air pollutants are emitted from different sources such as combustion byproducts, cooking, construction materials, office equipment, consumer products, and nearby traffic vehicles. BTEX is one group of major VOCs found in the indoor environments in Hong Kong and Mainland of China. In these areas, the concentration of BTEX was found in the range of 10-100 ppbv (Ao et al., 2003a). For example, recent studies in Hong Kong determined that the maximum concentration of BTEX in several selected shopping malls was 13.2, 78.1, 17.2, and 8.49 ppbv, respectively, while that in the selected office buildings was 2.51, 5.68, 6.40, and 13.0 ppbv, respectively. These studies indicated that the concentration of benzene in the shopping malls exceeded the criteria of IAQ in good class (5 ppb for benzene, HKEPD 2003).

Photocatalytic oxidation has proven to be a promising technology for air purification and may be more cost-effective than other conventional techniques such as activated carbon adsorption and chemical scrubbers, because semiconductors are inexpensive and capable of mineralizing most organic compounds effectively. However, this technique is still in the developmental stage for VOCs removal from indoor air (Fu et al., 1995; Ku et al., 2001; Feitz et al., 2002; Kim and Hong., 2002; Li et al., 2004). The bottle-neck is the development of a better catalyst. A good photocatalyst depends strongly on the efficiency of electron-hole pair separation and the adsorption ability of gaseous VOCs. To effectively eliminate the electron-hole recombination in the photocatalytic reaction, TiO_2 catalysts can be improved by doping some metal ions, coupling with other semiconductor oxides or

depositing noble metals (Choi et al., 1994; Li et al., 2001). However, some literature have proved that the incorporation of lanthanide ions such as La^{3+}, Eu^{3+}, Pr^{3+}, Nd^{3+}, and Sm^{3+} into TiO_2 matrix could promote the chemical or physical adsorption of organic substrates on the catalysts surface in an aqueous phase (Xu et al., 2002; Ranjit et al., 2001a and 2001b). In the meantime, this lanthanide ion doping could also improve the photochemical properties by increasing the photocurrent response and the incident monochromatic photon to current conversion efficiency in the light wavelength of 300-400 nm (Wang et al., 1999). The increase of photocurrent implies the effective separation of electron-hole pairs. In fact, the transient absorption decay spectra showed more effective separation of charge carriers for Gd^{3+} or Sm^{3+}-doped TiO_2 than for naked TiO_2 (Xu et al., 2002). However, the relevant information regarding the application of lanthanide ion-doped TiO_2 catalysts in gaseous reaction has been hardly reported based on the best of our knowledge. In reality, indoor air often contains BTEX with NO together (Jones, 1999). Concurrent photodegradation of BTEX and NO was also conducted. This study was aimed at applying the photocatalytic oxidation using the lanthanide ion-doped TiO_2 catalysts to remove VOCs from a gaseous stream for indoor air purification.

2. Experimental Methods

2.1 Preparation of Ln^{3+}-TiO_2 Catalysts

Two types of lanthanide ion-doped TiO_2 (Ln^{3+}-TiO_2) catalysts were prepared by doping La^{3+} or Nd^{3+} onto TiO_2 using a sol-gel process. 17 mL of tetra-n-butyl titanium (Ti(O-Bu)$_4$) was dissolved in 80 mL of absolute ethanol and the Ti(O-Bu)$_4$ solution was added drop-wise under vigorous stirring into 100 mL of a mixture solution containing 84 mL of 95% ethanol, 1 mL of 0.1 M Ln^{3+} (La(NO$_3$)$_3$·6H$_2$O and Nd(NO$_3$)$_3$·6H$_2$O, and 15 mL of acetic acid (> 99.8%). The resulting transparent colloidal suspension was stirred for 2 h and aged for 2 d till the formation of gel. The gel was dried at 353 K under vacuum and then ground. The powder was calcined at 773 K for 2 s, and eventually the Ln^{3+}-TiO_2 catalysts were obtained in a nominal atomic doping level of 0.2% abbreviated as 0.2% Ln^{3+}-TiO_2. Other lanthanide ion-doped TiO_2 samples prepared according to the

above procedure with the dosage of 0.7%, 1.2%, 1.6%, and 2.0%, respectively. In the meantime, pure TiO$_2$ as a blank catalyst was also prepared in the same way without doping lanthanide ions.

2.2 Characterization of Ln^{3+}-TiO$_2$ catalysts

To determine the crystal phase composition of the prepared Ln^{3+}-TiO$_2$ catalysts, X-ray diffraction (XRD) measurement was carried out at room temperature using a Rigaku D/MAX-IIIA diffractometer with CuK$_\alpha$ radiation (λ = 0.15418 nm). The accelerating voltage of 35 kV and emission current of 30 mA were used. The specific surface area, t-plot total surface area, t-plot surface area, monolayer volume, micropore surface area, and total pore volume of all samples were measured by the Brunauer-Emmett-Teller (BET) method, in which the N$_2$ adsorption at 77 K was applied and a Carlo Erba Sorptometer was used. To study the valance state and chemical state of the catalysts, X-ray photoelectron spectroscopy (XPS) was recorded with the PHI quantum ESCA microprobe system, using the MgK$_\alpha$ line of a 250-W Mg X-ray tube as a radiation source with the energy of 1253.6 eV, 16 mA × 12.5 kV and a working pressure of lower than 1×10^{-8} N m^{-2}. As an internal reference for the absolute binding energies, the C (1s) peak at 284.80 eV of hydrocarbon contamination was used. The fitting of XPS curves was analyzed with a software package (Multipak 6.0A). To study the recombination of electrons and holes, the photoluminescence (PL) emission spectra of the samples were measured with the following procedures: at 77 K, a 325 nm He-Cd laser was used as an excitation light source; The light from the sample was focused into a spectrometer (Spex500) and detected by a photo-multiplier tube (PMT); The signal from the PMT was inputted into a photon counter (SR400) before recorded by a computer.

2.3 Experimental Setup and preparation of gas streams

Different TiO$_2$ catalysts were first diffused into distilled water to make 5% (w/w) suspensions, and then dropped and coated on a glass microfiber filter (EPM2000) from Whatman International Ltd. as a supporting medium over an area of 20 cm × 21 cm (denoted as TiO$_2$ filter). It

was then calcinated at 120°C for 1 h with a temperature gradient of 5.5°C per minute from room temperature. The amount of imposed catalysts was determined by the weight difference before and after the coating procedure. In all experiments, the weight of all imposed catalysts was kept to be 1.64 g ± 5%.

A detailed experimental setup to carry out the photocatalytic oxidation reaction in a continuous gas flow reactor system is shown in Fig. 1. A photoreactor was used in this study, which had an effective volume of 18.6 L (20.1 [H] × 44.2 [L] × 21 [W] cm) and its surface was coated with a Teflon film (BYTAC Type AF-21). Illumination was provided by a 6-W UV lamp (Cole-Parmer EW-09815-41). The UV lamp with a primary emission at the wavelength of 365 nm was horizontally placed at the upper part of the reactor about 14 cm from both sides. The catalyst-coated filter was horizontally positioned below the UV lamp with a vertical distance of 5 cm. The light intensity on the catalyst surface was determined by a UV meter (Spectroline DRC-100X, 365nm detector) to be 750 μW cm^{-2}, which was applied throughout all the experiments in this study. Stainless steel sampling ports and Teflon tubing were used to connect the reactor and the analytical instruments.

A compressed gas cylinder from Spectra Gases Inc. containing benzene, toluene, ethyl-benzene, and *o-x*ylene (BTEX) with a mixing ratio of 1:1:1:1 at a concentration of 1 ppmv ± 2% for each component and a NO gas cylinder from BOC Gases Inc. with a concentration of 50 ppmv ± 2% were used as reactant gas sources, which complied with the traceable standard of National Institute of Standards and Technology. A zero air generator (Thermo Environmental Inc. Model 111) was used as an air gas source and the desired humidity of air gas flow was controlled from 2,100 to 22,000 ppmv by passing the zero air gas through a humidification chamber. The reactant gases and the zero air gas were mixed using different mass flow controllers (Advanced Pollution Instrumentation Inc. Model 700) to form a gas stream. The gas streams were pre-mixed by a gas blender and a desired flow rate was controlled at 15.5 L min^{-1}. The concentration of BTEX and NO

used in this study was 23±2 ppb and 190±5 ppb, respectively. Prior to the experiment, the adsorption had reached equilibrium after 60 min. Then, the UV lamp was turned on and the reaction was commenced (Ao and Lee, 2003; Ao et al., 2003b). The gas samples were collected at different time intervals. To obtain reliable results, all experiments were repeated 4 times and the averaged values were counted.

[FIG. 1]

2.4 Analyses

Pre-cleaned Summa canisters were used for VOCs sampling. During each experiment, several VOCs samples were collected at designated times and the sampling time was controlled by a mass flow controller. After collection, the canister sample was first concentrated by a Nutech Cryogenic Concentrator (Model 3550A), and the trapped VOCs were separated and analyzed by Hewlett Packard gas chromatograph (Model HP 6890) with a GC column from J & W Scientific Inc. and a mass selective detector (Model HP5973). After the analysis, the canister was sequentially evacuated and pressurized with humidified Zero air until all compounds detected had a concentration lower than 0.2 ppbv. TO-14 (Toxi-Mat-14M certified by Matheson) standard gas was analyzed using the GC/MS system seven times at 0.2 ppbv to obtain the method detection limits (Ao and Lee, 2003; Ao et al., 2003b).

The concentrations of NO, NO_2, and NO_x were continuously measured by a Chemiluminescence NO analyzer (Thermo Environmental Instruments Inc. Model 42c) at a sampling rate of 0.7 L min^{-1}. The NO analyzer was calibrated after each set of experiment. Calibration was performed through a Teflon sample line filter, which was also used during analysis. The flowrate for calibration was greater than the total flow required by the analyzer and any other flow demand connected to the manifold. The NO analyzer was allowed to sample zero air unit a stable reading was obtained. Then, span adjust was achieved be selecting the desire NO concentrations. The response of the NO analyzer was plotted against the corresponding NO concentrations. The experimental points

6

were connected using a straight line and determined by linear regression techniques. A minimum R^2 value of not less than 0.98 was achieved for all experiments.

3. Results and Discussion

3.1 Crystal Properties

The prepared Ln^{3+}-TiO_2 catalyst samples were first analyzed by XRD and the analytical results showed that all samples had a similar pattern of XRD grams, being dominated by anatase. From the XRD data, the crystallite sizes of the TiO_2 and Ln^{3+}-TiO_2 samples were calculated using the Scherrer formula and the results are shown in Table 1. These results showed that the crystallite sizes of both the La^{3+}-TiO_2 and Nd^{3+}-TiO_2 catalysts decreased owing to the Ln^{3+} doping. It may indicate that the lanthanide ion doping could hinder the increase of crystallite size during calcinations. In fact, the ionic radii of La^{3+} and Nd^{3+} are 1.15 and 0.99 Å, respectively, which are bigger than that of Ti^{4+} (0.68 Å). It seems not possible for these lanthanide ions to really enter the lattice of TiO_2 structure. Xu et al. (2002) thought that lanthanide ion could not get into the lattice of TiO_2 to replace Ti^{4+} ion; on the contrary, on the interface of Ln^{3+}-TiO_2, Ti^{4+} ion might substitute for lanthanide ions in the lattice of lanthanide oxides and a Ti-O-Ln bond could be formed. Shah et al. (2002) proposed that Nd^{3+} resides in the octahedral interstitial site for Nd^{3+}-TiO_2 and the high oxygen affinities of interstitially locating neodymium ion effectively either create a localized positive charge around Ti or form an oxygen vacancy. It would rather be believed that the lanthanide ion inside in the octahedral interstitial site because of a lower dosage in this study. However, whatever Ti^{4+} replaces Ln^{3+} or lanthanide ions inside in the octahedral interstitial site, it will make an unbalanced charge. The formation of Ti-O-Ln bond and the charge imbalance might influence the surface chemical state of Ln^{3+}- TiO_2 greatly.

[Table 1]

3.2 BET analyses

The specific surface area, t-plot total surface area, t-plot surface area, monolayer volume, micropore surface area, and total pore volume of TiO_2 and Ln^{3+}-TiO_2 samples were measured by the BET method and the results are also listed in Table 1. The BET results showed that surface area except for micropore surface area increased significantly, owing to the Ln^{3+} doping. Especially, the 0.7% Ln^{3+}-TiO_2 samples had the largest micropore surface area, the micropore volume, and also the total pore volume.

To investigate the effects of lanthanide ion doping on the pore structure and adsorption abilities of the TiO_2 catalyst, a set of nitrogen adsorption/desorption isotherm tests was carried out and the experimental results are presented in Fig. 2. The pore-size distribution of the different catalysts was also determined by Barrett-Joyner-Halenda method and is expressed in Fig. 3. The adsorption isotherms in Fig. 2 demonstrated a pattern of Type IV curves (Gregg and Sing, 1982), which is a typical feature of porous materials. It can be seen that all the lanthanide ion-doped TiO_2 catalysts had higher adsorption capacity than the TiO_2 catalyst. Among them, the 0.7% Ln^{3+}-TiO_2 samples achieved the highest value for both the La^{3+}-TiO_2 and Nd^{3+}-TiO_2 catalysts. However, the La^{3+}-TiO_2 samples demonstrated that the adsorption ability decreased from its peak value clearly, when the La^{3+} dosage exceeded 0.7%. In the meantime, the well defined hysteresis loops in Fig. 2 confirmed that all the samples had a disorderd mesoporous structure, which was attributed to pores formed between TiO_2 particles (Yu et al., 2001; 2003a; 2003b). These hysteresis loops of the Ln^{3+}-TiO_2 demonstrated a curve pattern between Type H1 and Type H2 (Gregg and Sing, 1982) while that of TiO_2 showed Type H2. Type H1 loops are often obtained with agglomerates or compacts of spherical particles of uniform size array while the distribution of pore size and shape might not be well defined for Type H2 loops. The results as shown in Fig. 3 demonstrated that the pore sizes of most catalysts were distributed in the range of 4-16 nm, in which the pure TiO_2 catalyst had a dominant pore size of 3.65-14.54 nm; the 0.7, 1.2, and 2.0% La^{3+}-TiO_2 samples had pore sizes of

4.01-13.93, 3.65-11.29, and 3.65-9.15 nm; and the 0.7, 1.2, and 2.0% Nd^{3+}-TiO_2 samples had their pore sizes of 3.65-14.05, 3.65-12.33, and 3.65-10.01 nm, respectively. The analytical results demonstrated that the percentage of pore volume with the sizes of 3.65-5.79, 5.79-9.15, and 9.15-14.54 nm was 4.3, 77.1, and 18.5%, respectively for TiO_2; the percentage of pore volume with the sizes of 4.01-5.17, 5.17-12.33, and 12.33-16.01 nm was 8.0, 90.4, and 1.6% respectively for 0.7% La^{3+}-TiO_2; the percentage of pore volume with the sizes of 3.65-5.17, 5.17-11.29, and 11.29-16.01 nm was 3.0, 95.4, and 1.6%, respectively for 1.2% La^{3+}-TiO_2, and the percentage of pore volume with the sizes of 3.65-5.17, 5.17 -9.15, 9.15-16.01 nm was 7.3, 89.7, and 3.0% respectively for 2.0% La^{3+}-TiO_2. Similar results were also obtained for the Nd^{3+}-TiO_2 catalysts. These results indicated that the Ln^{3+}-TiO_2 catalysts had a quite uniform pore size and its size distribution followed a normal distribution pattern like the Type H1 loop. Obviously, the 0.7% Ln^{3+}-TiO_2 samples had the highest pore size and the maximum pore volume,

[FIG. 2]

[FIG. 3]

3.3 The Photocatalytic Degradation of BTEX with Different Catalysts

A set of experiments to photocatalytic degrade BTEX in a gaseous phase was carried out in the continuous flow reactor system using different catalysts. A gas stream containing 4 components of benzene, toluene, ethyl-benzene, and *o-x*ylene with an initial concentration of 23 ± 2 ppbv and a humidity level of 15,700 ppmv passed through the reactor at a flow rate of 15.5 L min^{-1} with an empty bed retention time of 72 s. After a stabilized period of about one hour, the BTEX concentrations in the outlet gas became as same as that in the inlet gas and the experiment commenced by turning on the UV lamp. Each of experiments lasted for 4 h, in which 6 gas samples were collected at the designated time intervals of 10, 20, 60, 90, 120, and 240 min, respectively. The experimental results of BTEX reduction against experimental time are shown in Figs. 4(a), 4(b), 4(c), and 4(d). It can be seen that the concentration of BTEX dropped rapidly in the first 20 min and then

9

reached a steady concentration after 120 min gradually. The removals of 4 components using different catalysts quantified out based on the data obtained in the steady state of each experiment and are shown in Figs. 5a and 5b. The results showed that the BTEX removals with TiO_2 were 4.80, 13.7, 21.2, and 45.8%, respectively. Then, the BTEX removals increased with the doping amount of lanthanide ions significantly and the 1.2% Ln^{3+}-TiO_2 catalyst achieved the highest BTEX removals of 29.7, 58.4, 70.4, and 78.8% (1.2% La^{3+}-TiO_2) and 22.6, 43.1, 64.3, and 71.1% (1.2% Nd^{3+}-TiO_2). These results indicated that the 1.2% of lanthanide ion doping could be an optimum amount in this experimental condition.

It is generally believed that the efficiency of photocatalytic degradation depends on both the adsorption ability and photocatalytic activity of catalysts. In this study, the experimental results showed that the 0.7% Ln^{3+}-TiO_2 samples had the highest N_2 adsorption ability (Fig. 2), but the 1.2% Ln^{3+}-TiO_2 catalysts achieved the highest BTEX removals. The BTEX removals affected by different doping dosage are compared in Figs. 5a and 5b. It can be seen that the 1.2% La^{3+}-TiO_2 catalysts performed better than the 1.2% Nd^{3+}-TiO_2 catalysts significantly. In the meantime, the experiments also demonstrated that both the 1.2% Ln^{3+}-TiO_2 catalysts performed much better than a representative TiO_2 catalyst (Degussa P-25) as shown in Fig. 6a.

Among the four VOCs, *o*-xylene had the highest removal and benzene had the lowest removal. Similar photodegradation patterns were also observed using a higher initial concentration at ppmv levels (Hennezel and Ollis, 1997). The different removal rates of BTEX under the same reaction condition could result from both reasons: the different adsorption rates of BTEX on the catalyst surface reported by Larson and Falconer (1997) and the more rapid rate of hydroxyl radicals reacting with *o*-xylene, followed by ethylbenzene, toluene and benzene under atmospheric environment (Ao and Lee, 2003; Ao et al., 2003b).

[FIG. 4]

[FIG. 5]

3.4 The Photocatalytic Degradation of BTEX affected by Humidity and NO

The BTEX photocatalytic degradation reaction was also conducted at different humidity levels from 2,100 to 22,000 ppmv. The experiments using 1.2% Nd^{3+}-TiO_2 with a BTEX initial concentration of 23 ± 2 ppbv and a residence time of 72 s was carried out for 4 h at different humidity levels and the experimental results are shown in Fig. 6b. The results showed that BTEX removals significantly decreased with the increase of the humidity levels. At the humidity of 2,100 ppmv, the conversion of benzene, toluene, ethylbenzene, and *o*-xylene were 27, 67, 76, and 80%, respectively. However, as humidity increased to 22,000 ppmv, the BTEX removals significantly dropped to 2, 15, 28, and 35%, respectively. These results clearly indicated that high humidity levels would inhibit the conversion of BTEX. The same results had been reported by using the P-25 catalyst (Ao et al., 2003a and 2003b; Ao and Lee, 2003;). On the contrary, it was also reported that the conversion of toluene, benzene, and *m*-xylene at a ppmv level increased with the increase of humidity level (Peral and Ollis, 1992; Hennezel et al., 1998). In fact, Obee and Brown (1995) reported that the optimum humidity level for the toluene photocatalytic removal strongly depended on its initial concentration as well. Generally, water molecular takes part in photocatalytic reaction and the presence of water would promote the formation of hydroxyl radicals. In the meantime, for gaseous photocatalytic reaction, water vapor would compete with the adsorption site on the TiO_2 surface and make the adsorption of VOCs decrease. When the concentration of water vapor reaches a certain value, the formation of hydroxyl radicals would not increase with the increase of water vapor and the adsorption of VOCs keep decreasing with the increase of water vapor. Therefore, it was not surprising that the conversion of BTEX decreased with the increase of humidity level in our experiments, but unfortunately an optimum humidity level could not be determined in this study because it was difficult to adjust a humidity level below 2,100 ppmv in our laboratory conditions.

[FIG. 6]

Fig. 7 demonstrated that existence of NO only slightly promoted the BTEX removals in the presence of NO with the concentration of 190 ± 5 ppbv and with a residence time of 72 s and humidity level of 2,100 ppmv by using the 1.2% La^{3+}-TiO_2 catalyst. With NO in the experiments, benzene, toluene, ethylbenzene, and o-xylene were removed by 36, 80, 85, and 89% respectively, compared to that without NO by 36, 79, 82, and 85% at the humidity level of 2,100 ppmv. Since the hydroxyl radicals were generated during the photodegradation of NO, they could react with BTEX and enhanced their conversion (Ao et al., 2003a). However, the conversion of benzene, toluene, ethylbenzene, and o-xylene also dropped rapidly to 2.9, 5.9, 27 and 41% respectively with NO when the humidity level increased up to 22,000 ppmv.

[FIG. 7]

In the above experiment, three concentrations of NO, NO_2 and NO_x were monitored simultaneously and the results are shown in Fig. 8. It could be clearly seen that the NO concentration dropped rapidly within the first few minutes and reached a steady concentration after few minutes in the experiment. Once the NO reduced significantly, up to 10 ppb of NO_2 as a by-product of NO oxidation was detected in the experiment. It was also found that at the humidity level of 2,100 ppmv, a residual concentration of NO around 19 ppbv after 5 min had been maintained until the end of experiment. This result indicated a rapid deactivation of the photocatalyst during the NO photodegradation. In the meantime, it was found that the NO_2 concentration was increased from 5 ppbv at 5 min to 10 ppbv at 40 min and then kept no further change. At the end of experiment, the concentration of NO_x was determined to be around 29 ppbv and the NO was eventually removed by 85%.

[FIG. 8]

3.5 The Mechanisms of BTEX Degradation Enhancement by Using Ln^{3+}-TiO_2 Catalysts

The efficiency of BTEX photocatalytic degradation strongly depends on the adsorption properties and the photocatalytic activity of the catalysts, which are affected by their crystal composition, surface chemical states and valence band structure. Our research group had reported that the adsorption equilibrium constant of the Ln^{3+}-TiO_2 catalysts for the 2-mercaptobenzothiazole adsorption in an aqueous phase increased with the increase of lanthanide ion dosage because of the chemical adsorption between lanthanide ions and –SH group of 2-mercaptobenzothiazole molecular structure (Li et al., 2004). However, the adsorption of BTEX in this study was dominated by physical adsorption. The data from the BET analysis might be useful to interpret the effect of lanthanide ion doping on the adsorption of BTEX. According to nitrogen adsorption-desorption isotherms and pore size distribution, the 0.7% Ln^{3+}-TiO_2 catalysts had the highest adsorption ability, but the 1.2% Ln^{3+}-TiO_2 catalysts achieved the best performance for BTEX removals. These information may imply that the 1.2% Ln^{3+}-TiO_2 catalysts had better photocatalytic activity by separating electron-hole pairs more efficiently, which played a more significant role than the adsorption ability. In our investigation, the crystal composition of all catalysts was quite similar, which should not make any significant difference in their photocatalytic activity. Alternatively the modification of the surface state and valence band structure of the catalysts might be another critical reason for promoting the photocatalytic activity. Ranjit et al.(2001a and 2001b) reported that the formation of a hetero-junction between TiO_2 and lanthanide oxides could not prevent electron-hole recombination because the conduction band edges of lanthanide oxides lie at a far more negative position (about -1.8 to -3.5 eV vs. standard hydrogen electrode (SHE) than that of TiO_2 (about -0.3 V vs. SHE for anatase). In fact, Wang and his co-workers (1999) had proved the more efficient separation of electron-hole pairs in La^{3+}-TiO_2 and Nd^{3+}-TiO_2 than in pure TiO_2. In this study, the optimal dosage of lanthanide ion was found to be 1.2% due to the fact that this dosage achieved the most efficient separation of electron-hole pairs, owing to the formation of Ti^{3+} and the introduction of lanthanide crystal field state. The formation of Ti^{3+} had also been confirmed by Liu et al. (2003). Those studies indicated that the charge imbalance caused by titanium entering into the lattice of lanthanum oxide during heat

treatment made Ti^{4+} reduced to Ti^{3+}. Also the XPS data in the studies showed that the amount of Ti^{3+} existing on the surface of photocatalysts increased with the increase of lanthanum ion dosage. Moreover, our previous investigation (Liu et al. 2003) indicated that a limited amount of oxygen defect sites (OV) and Ti^{3+} species generated during the H_2 reduction appear as the defects in the TiO_2 structure. While the electrons and holes are generated in the initial stage of UV illumination, the defects on the TiO_2 surface or in the bulk solution can suppress the recombination of electron-hole pairs and hence extend their lifetime (Linsebiger et al. 1995). The OV and Ti^{3+} species act as hole traps. Once the OV and Ti^{3+} are combined with the holes, they become charged species. At the same time, oxygen acts as electron traps during the reaction. At the meantime, Ti^{3+} on the surface is oxidized by molecular oxygen to form the superoxide anion and holes trapped by superoxide anion lead to the formation of OH radical (Shah et al., 2002). At some degree, the higher content of Ti^{3+} on the surface of the La^{3+}-TiO_2 would be one of the significant reasons to change their photoactivity. However, there must be an optimum content of Ti^{3+} existing on the La^{3+}-TiO_2. Although the 2.0% La^{3+}-TiO_2 had a higher content of Ti^{3+} than that of 1.2% La^{3+}-TiO_2, its photoactivity was lower than that of 1.2% La^{3+}-TiO_2 in this study. Therefore, Ti^{3+} acts as the charge-carrier recombination centre, and advances the recombination of electron-hole pairs, and then the photoactivity may decrease. Therefore, the presence and the optimal content of Ti^{3+} might be the critical factor leading the improvement of BTEX photocatalytic degradation for La^{3+}-TiO_2. On the other hand, Frindell's group (2003) proposed a model for energy transfer involving relaxation to defect states on TiO_2 and then to the lanthanide ions for a lanthanide ion-doped TiO_2 system and the defect states played an important role in energy transfer and electron transfer between host (TiO_2) and guest (Ln^{3+}). Xie and Yuan (2004) proposed that electron could transfer from conduction band of TiO_2 to neodymium cluster $(Nd)^{m+}$ for Nd^{3+}-TiO_2. To better understand the effect of lanthanide ion doping on the separation of electron-hole pairs, the PL emission spectra of TiO_2 and different Ln^{3+}-TiO_2 catalysts were examined in this study. The PL techniques have been given a great deal of attention in the field of photocatalysis over solid semiconductors as a useful probe for understanding the surface processes in which photogenerated electrons and holes takes part (Kelly et al., 1999). Radiative recombination of

14

electron and hole either directly (band-band) or indirectly (via a bandgap state) gives light emission (PL). PL is simply the optical excitation of a sample to create electron-hole pairs call exciton. PL emission mainly results from the recombination of excited electron and holes, the lower PL intensity may indicate a lower recombination rate of electron/holes and higher separation efficiency under the same test conditions (Kelly et al., 1999; Chamarro et al, 1996). In this study, the PL emission spectra of the TiO_2 and 1.2% Ln^{3+}-TiO_2 catalysts were examined in the range of 370-700 nm at a temperature of 77 K and the analytical results are shown in Fig. 9. The PL emission intensity of TiO_2 was more significantly stronger than that of Ln^{3+}-TiO_2. In addition, the PL emission peak for TiO_2 was located at 520 nm, but those for 1.2% La^{3+}/Nd^{3+}-TiO_2 located at 525 and 522 nm, respectively, attributable to the recombination of the host charge carrier. Therefore, it might be concluded that the separation efficiency of electron-hole pairs for 1.2% La^{3+}/Nd^{3+}-TiO_2 should be higher than for pure TiO_2. On the other hand, it was noticeable that some new PL emission peaks appeared at 502, 542, and 608 nm for 1.2% Nd^{3+}-TiO_2. To the best of our knowledge, there have not been any reports regarding the PL emission peaks between 400-700 nm attributable to the intra-4*f* shell transition of Nd^{3+} in any materials. And the *f-f* transitions are fairly insensitive to conditions such as temperature and the surrounding chemical environment. Therefore, these new peaks might be contributed to the energy transfer between neodymium ion and TiO_2. The PL emission spectra imply the fact that electron was transferred from TiO_2 to Ln^{3+} crystal field states. Hence, the presence of Ti^{3+} and lanthanide crystal filed states was the key factors in enhancing the separation efficiency of electron-hole pairs.

[FIG. 9]

4. Conclusions

The XRD results showed that the crystal size greatly decreased due to lanthanide ion-doping but an increase in specific surface area, t-plot total surface area, micropore volume, and the total pore volume was observed. The TiO_2-based photocatalysts had the mesoporous structure with 4-16 nm

pore size distribution by means of BET analysis. Nitrogen adsorption-desorption isotherms showed that the adsorption ability was enhanced owing to lanthanide ion doping and 0.7% Ln^{3+}-TiO_2 had the highest adsorption ability. The effect of lanthanide ion doping with different dosage on photocatalytic activity was investigated by performing the photodegradation of BTEX. The results showed the photocatalytic efficiency for BTEX removal was remarkably enhanced owing to lanthanide ion doping, and 1.2% Ln^{3+}-TiO_2 had the highest photocatalytic activity, which was much higher than P-25. Possible mechanisms of the enhanced activity could be due to both the increase of adsorption ability and the enhancement of electron-hole pairs separation, which was attributed to the presence of suitable amount of Ti^{3+} on the surface of Ln^{3+}-TiO_2 and the introduction of lanthanide crystal field states. BTEX photocatalytic removal efficiency was decreased with the increase of humidity level and increased owing to NO addition. By doping Ln^{3+} into TiO_2, the removal of BTEX increased significantly. Nevertheless, the removal of BTEX, especially at high humidity levels, is still not satisfied. We are currently modifying the photocatalyst so that it can be used at high humidity environment for cities located in the tropical zone such as Hong Kong.

References

Ao, C. H., Lee, S. C., Mak, C. L., Chan, L. Y., 2003a. Photodegradation of volatile organic compounds (VOCs) and NO for indoor air purification using TiO_2: promotion versus inhibition effect of NO. *Appl. Catal. B. Environ.* 42, 119-129.

Ao, C. H., Lee, S. C., Yu, J. C., 2003b. Photocatalyst TiO_2 supported on glass fiber for indoor air purification: effect of NO on the photodegradation of CO and NO_2. *J. Photochem. Photobiol. A: Chem.* 156, 171-177.

Ao, C. H., Lee, S. C., 2003. Enhancement effect of TiO_2 immobilized on activated carbon filter for the photodegradation of pollutants at typical indoor air level. *Appl. Catal. B Environ.* 44, 191-205.

Chamarro, M., Gourdon, C., Lavallard, P., 1996. Photoluminescence polarization of semiconductor nanocrystals. *J. Lumin.* 70, 222-237.

Choi, W., Termin, A., Hoffmann, M. R., 1994. The role of metal ion dopants in quantum-sized TiO_2: correlation between photoreactivity and charge carrier recombination dynamics. *J. Phys. Chem.* 98, 13669-13679.

Hennezel, O., Pichat, P., Ollis, D.F., 1998. Benzene and toluene gas-phase photocatalytic degradation over H_2O and HCl pretreated TiO_2: by-products and mechanisms. *J. Photochem. Photobiol. A: Chem.* 118, 197-204.

Feitz, A. J., Guan, J., Chattopadhyay, G., Waite, T. D., 2002. Photo-Fenton degradation of dichloromethane for gas phase treatment. *Chemosphere* 48, 401-406.

Frindell, K. L., Bartl, M. H., Robinson, M. R., Bazan, G. C., Popitsch, A., Stucky, G. D., 2003. Visible and near-IR luminescence via energy transfer in rare earth doped mesoporous titania thin films with nanocrystalline walls. *J. Solid State Chem.* 172, 81-88.

Fu, X., Zeltner, W. A., Anderson, M. A., 1995. The gas-phase photocatalytic mineralization of benzene on porous titania-based catalysts. *Appl. Catal. B. Environ.* 6, 209-224.

Gregg, S. L., Sing, K. S. W., 1982. *Adsorption, Surface Area and Porosity*, Academic Press, London.

HKEPD (Hong Kong Environmental Protection Department). *Guideline notes for the management of indoor air quality in offices and public places* . Indoor Air Quality Management Group, Hong Kong, 2003.

Hennezel, O., Ollis. D.F., 1997. Trichloroethylene-promoted photocatalytic oxidation of air contaminants. *J. Catal.* 167, 118-126.

Jones, A.P., 1999. Indoor air quality and health. *Atmos. Enviorn.* 33, 4535-4564.

Kelly, J. J., Kooij, E. S., Meulenkamp, E. A., 1999. Luminescence studies of semiconductor electrodes. *Electrochimica Acta* 45, 561-574.

Kim, S. B., Hong, S. C., 2002. Kinetic study for photocatalytic degradation of volatile organic compounds in air using thin film TiO_2 photocatalyst. *Appl. Catal. B. Environ.* 35, 305-315.

Ku, Y., Ma, C. M., Shen, Y. S., 2001. Decomposition of gaseous trichloroethylene in a photoreactor with TiO_2-coated nonwoven fiber textile. *Appl. Catal. B. Environ.* 34, 181-190.

Larson, S.A., Falconer, J. L., 1997. Initial reaction steps in photocatalytic oxidation of aromatics. *Catal. Lett.* 44, 57-65.

Li, F. B., Li, X. Z., Hou, M. F., 2004. Photocatalytic degradation of 2-mercaptobenzothiazole in aqueous La^{3+}–TiO_2 suspension for odor control. *Appl. Catal. B. Environ.* 48, 185-194.

Li, X. Z., Li, F. B., Yang, C.L., Ge, W.K., 2001. Photocatalytic activity of WO_x-TiO_2 under visible light irradiation. *J Photochem Photobiol A: Chem*. 141, 209-217.

Linsebiger, A.L., Lu, G.Q., Yates Jr., J.T., 1995. Photocatalysis on TiO_2 surfaces: principles, mechanisms, and selected results. *Chem. Rev.* 95, 735-758.

Liu, H., Ma, H. T., Li, X. Z., Li, W. Z., Wu, M., Bao, X. H., 2003. The enhancement of TiO_2 photocatalytic activity by hydrogen thermal treatment. *Chemosphere* 50, 39-46.

Maroni, M., Seifert, B., Lindvall, T. (Eds.), 1995. *Indoor Air Quality – a Comprehensive Reference Book.* Elsevier, Amsterdam.

Obee, T.N., Brown, R.T., 1995. TiO_2 Photocatalysis for indoor air applications: effects of humidity and trace contaminant levels on the oxidation rates of formaldehyde, toluene, and 1,3-butadiene. *Environ. Sci. Technol.* 29, 1223-1231.

Peral, J., Ollis, D.F., 1992. Heterogenous photocatalytic oxidation of gas-phase organics for air purification-acetone, 1-butanol, butyraldehyde, formaldehyde and meta-xylene oxidation. *J. Catal.* 136, 554-565.

Ranjit, K. T., Willner, I., Bossmann, S. H., and Braun, A. M., 2001a. Lanthanide oxide doped titanium dioxide photocatalysts: effective photocatalysts for the enhanced degradation of salicylic acid and *t*-cinnamic acid. *J. Catal.* 204, 305-311.

Ranjit, K. T., Willner, I., Bossmann, S. H., Braun, A. M., 2001b. Lanthanide oxide-doped titanium dioxide photocatalysts: novel photocatalysts for the enhanced degradation of *p*-chlorophenoxyacetic acid. *Environ. Sci. Technol.* 35, 1544-1549.

Roberts, J., Nelson. W.C., 1995. *National Human Activity Pattern Survey Data Base*. United States Environmental Protection Agency (USEPA), Research Triangle Park, NC.

Shah, S. I., Li, W., Huang, C.-P., Jung, O., Ni. C., 2002. Study of Nd^{3+}, Pd^{2+}, Pt^{4+}, and Fe^{3+} dopant effect on photoreactivity of TiO_2 nanoparticles. *Proc. Nat. Acad. Sci.* 99, 6482-6486.

Wang, Y. Q., Cheng, H. M., Hao, Y. Z., Ma, J. M., Li, W. H., Cai, S. M., 1999. Photoelectrochemical properties of metal-ion-doped TiO_2 nanocrystalline electrodes. *Thin Solid Films* 349, 120-125.

Xie, Y. B., Yuan, C. W., 2004. Photocatalysis of neodymium ion modified TiO_2 sol under visible light irradiation. *Appl. Surf. Sci.* 221, 17-24.

Xu, W., Gao, Y., Liu, H. Q., 2002. The preparation, characterization, and their photocatalytic activities of rare-earth-doped TiO_2 nanoparticles. *J. Catal.* 207, 151-157.

Yu, J. C., Yu, J. G., Ho, W. K., Zhang, L. Z., 2001. Preparation of highly photocatalytic active nano-sized TiO_2 particles via ultrasonic irradiation. *Chem. Commun.* 1942-1943.

Yu, J. G., Yu, J. C., Leung, M. K.-P., Ho, W. K., Cheng, B., Zhao, X. J., Zhao, J. C., 2003a. Effect of acidic and basic hydrolysis catalysts on the photocatalytic activity and microstructure of bimodal mesoporous titania. *J. Catal.* 217, 69-78.

Yu, J. G., Yu, J. C., Cheng, B., Hark, S. K., Iu, K., 2003b. The effect of F⁻-doping and temperature on the structural and textural evolution of mesoporous TiO_2 powders. *J. Solid State Chem.* 174, 372-380.

Table 1. Crystal parameters and BET data of TiO_2 and Ln^{3+}-TiO_2 catalysts

Photocatalysts	Pure TiO₂	La³⁺-TiO₂			Nd³⁺-TiO₂		
		0.7%	1.2%	2.0%	0.7%	1.2%	2.0%
Crystal pattern	A*	A*	A*	A*	A*	A*	A*
Crystal size (nm)	32.9	22.9	17.7	17.6	19.2	19.80	17.8
The specific surface area (m^2 g^{-1})	50.20	73.87	83.81	76.42	71.25	78.54	90.81
t-plot total surface area (m^2 g^{-1})	55.94	81.60	83.81	86.33	79.09	88.68	90.81
t-plot surface area (m^2 g^{-1})	51.94	75.00	78.78	82.80	72.38	82.92	85.78
Monolayer volume (cm^3 g^{-1}, STP)	11.53	16.97	19.25	17.55	16.36	18.04	20.86
Micropore surface area (m^2 g^{-1})	4.00	6.60	5.03	3.53	6.71	5.76	5.03
Micropore volume (10^{-3} cm^3 g^{-1})	1.13	2.06	1.15	0.51	2.17	1.53	1.26
The total pore volume (cm^3 g^{-1}) ($P_s/P_0 = 0.9814$, adsorption)	0.152	0.270	0.228	0.205	0.252	0.248	0.234

*A = anatase

FIG. 1. Schematic diagram of the experimental set-up

FIG. 2. Nitrogen adsorption/desorption isotherms of La^{3+}-TiO_2 catalysts (a) and Nd^{3+}-TiO_2 catalysts (b) vs. lanthanide ion dosage.

FIG. 3. Pore-size distribution of La^{3+}-TiO_2 catalysts (a) and Nd^{3+}-TiO_2 catalysts (b) vs. lanthanide ion dosage.

FIG. 4. Photocatalytic degradation of benzene (a), toluene (b), ethylbenzene (c), and *o-x*ylene (d) in the continuous gas flow reactor with an initial concentration: 23 ± 2 ppbv, residence time: 72 s, and humidity level: 15700 ppmv by using TiO_2 and La^{3+}-TiO_2 photocatalysts.

FIG. 5. Photocatalytic removal percentage of benzene, toluene, ethylbenzene and *o-x*ylene in the continuous gas flow reactor with an initial concentration: 23 ± 2 ppbv, residence time: 72 s, and humidity level: 15700 ppmv by using La^{3+}-TiO_2 (a) and Nd^{3+}-TiO_2 (b) photocatalysts.

FIG. 6. Photocatalytic removal percentage of benzene, toluene, ethylbenzene, and *o-x*ylene in the continuous gas flow reactor with an initial concentration: 23 ± 2 ppbv, residence time: 72 s by suing different catalysts at a same humidity level: 15,700 ppmv (a), and by using 1.2% Nd^{3+}-TiO_2 at different humidity levels: 2,100 ppmv, 15,700 ppmv and 22,000 ppmv (b).

FIG. 7. Effects of NO_x addition and humidity level on the removal percentage of benzene, toluene, ethylbenzene, and *o-x*ylene in the continuous gas flow reactor, with an initial concentration: 23 ± 2 ppbv, residence time: 72 s by using 1.2% La^{3+}-TiO_2 catalyst.

FIG. 8. Photocatalytic removal of NO_x with an initial concentration: 190±5 ppbv in the BTEX stream with a BTEX initial concentration: 23±2 ppbv; residence time: 72 s. and humidity level: 2,100 ppmv.

FIG. 9. Photoluminescence emission spectra of TiO_2, 1.2% La^{3+}-TiO_2, and 1.2% Nd^{3+}-TiO_2 catalysts at temperature: 77 K, wavelength: 350 - 700 nm.

Fig. 1

1. Zero air generator chamber   2. Humidification chamber
3. Standard gas   4. Calibrator
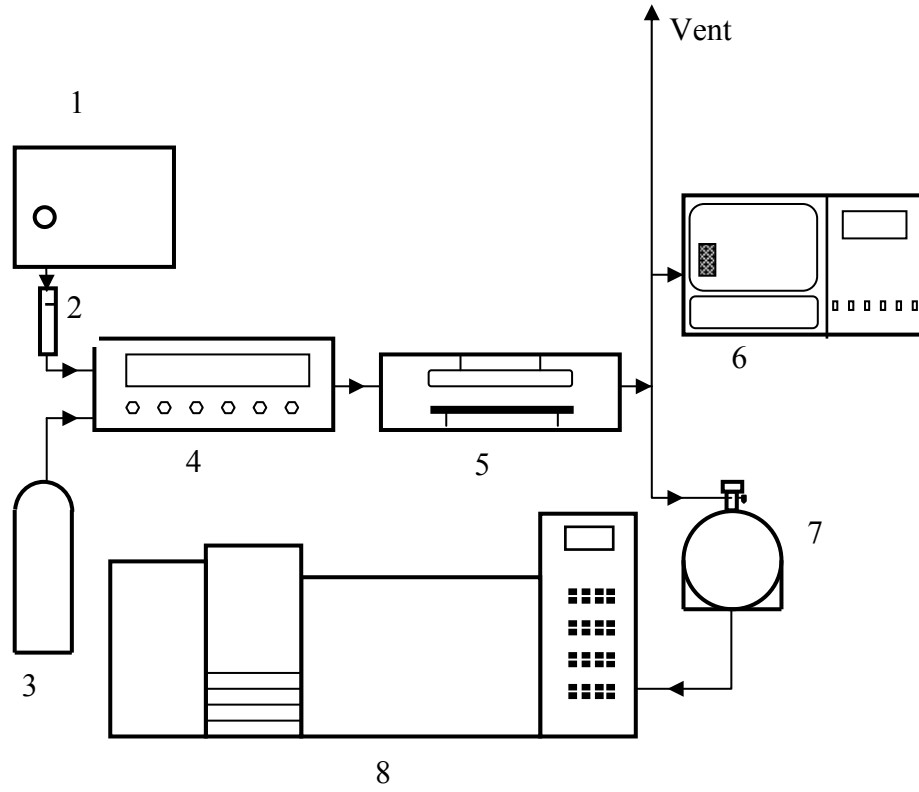5. Photoreactor   6. NOx analyzer
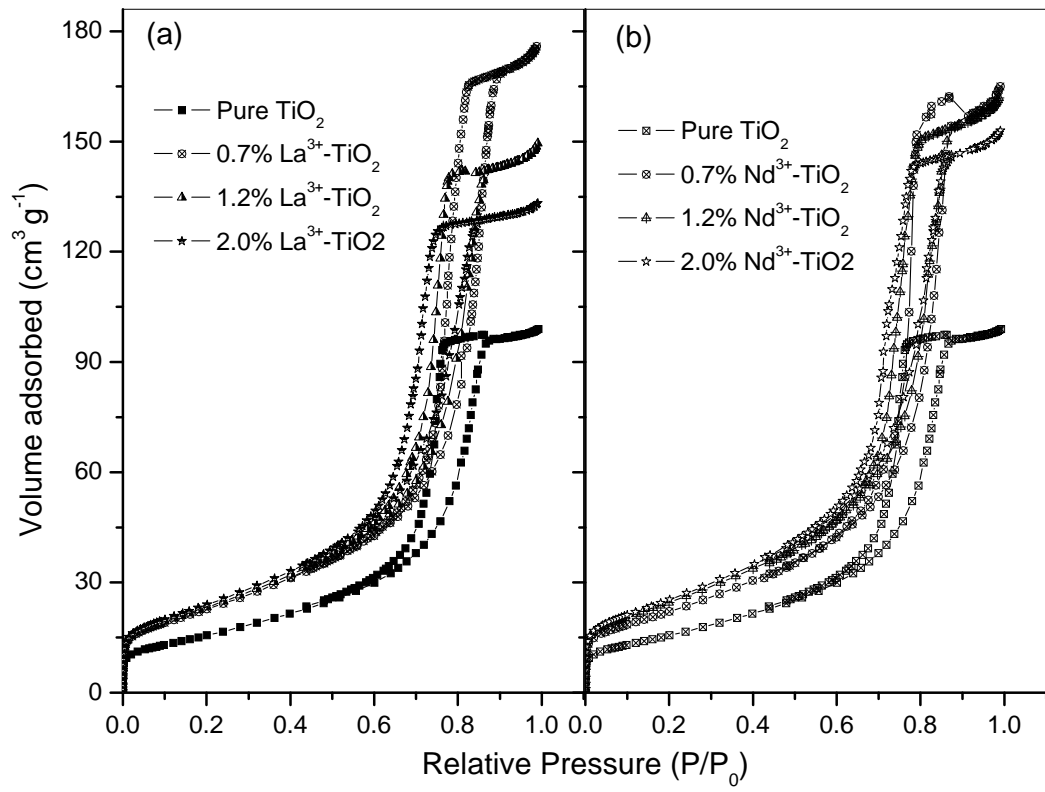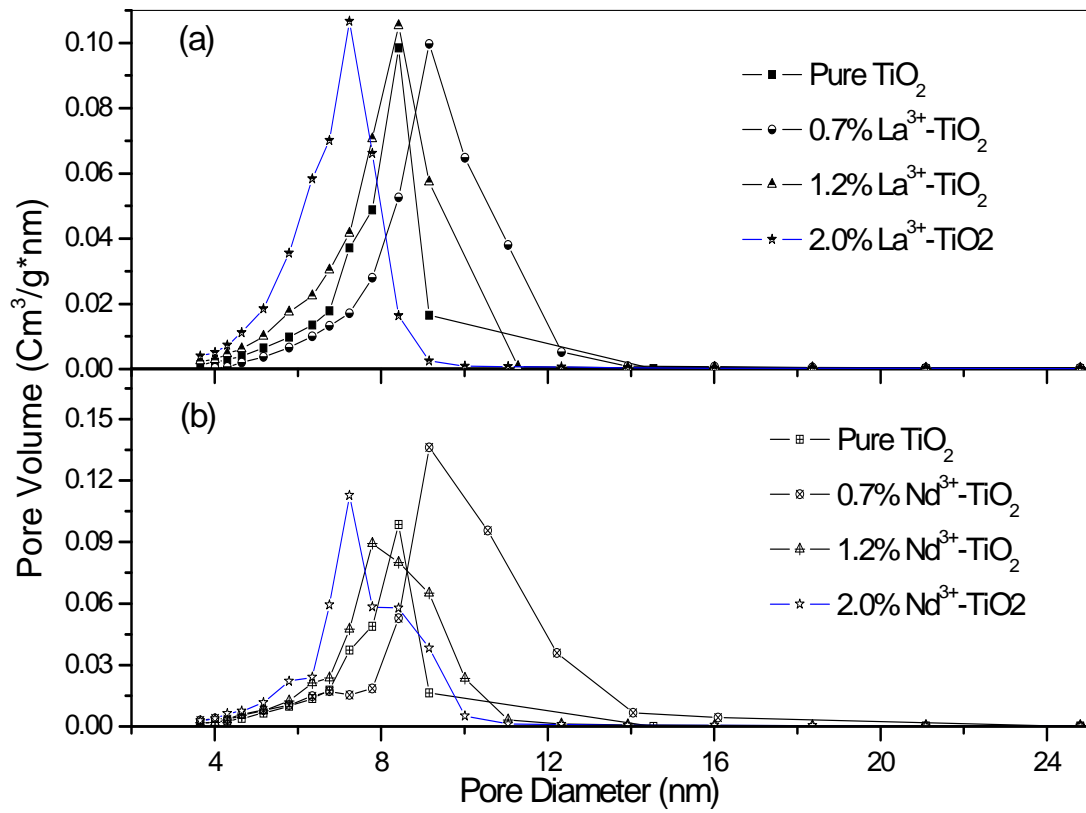7. Summa canister   8. GC/MS
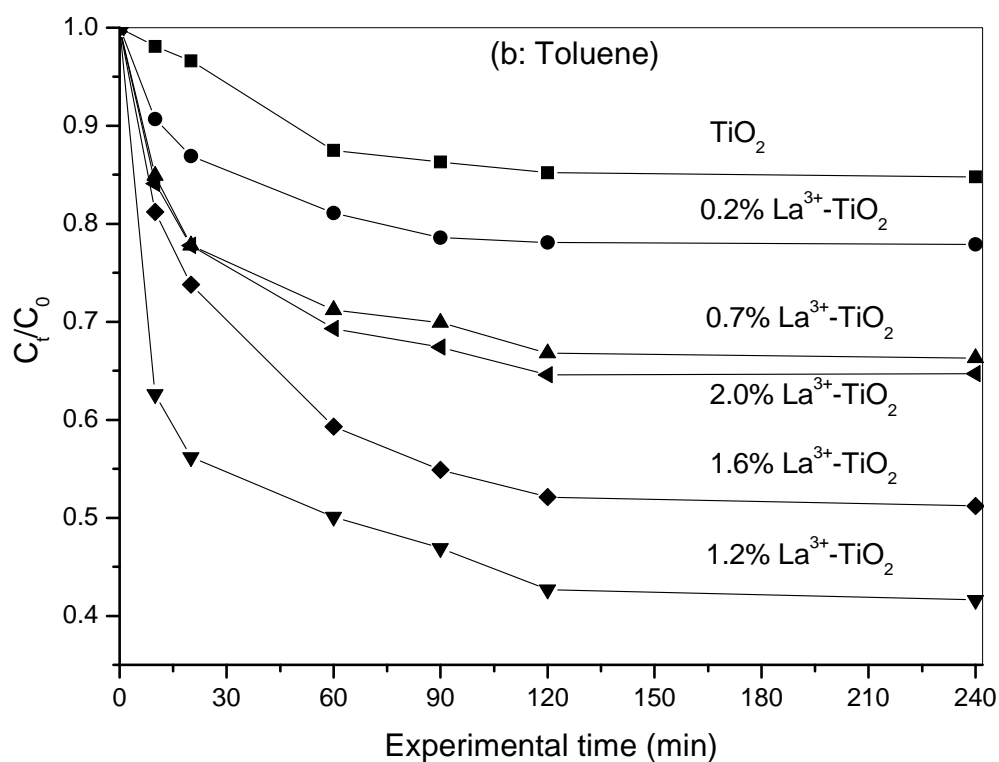
Fig. 2

Fig. 3

FIG. 4

(c: ethylbenzene)

TiO$_2$

0.2% La^{3+}-TiO$_2$

0.7% La^{3+}-TiO$_2$

2.0% La^{3+}-TiO$_2$

1.6% La^{3+}-TiO$_2$

1.2% La^{3+}-TiO$_2$

C$_t$/C$_0$

Experimental time (min)

(d: o-xylene)

TiO$_2$

0.2% La^{3+}-TiO$_2$

0.7% La^{3+}-TiO$_2$

2.0% La^{3+}-TiO$_2$

1.6% La^{3+}-TiO$_2$

1.2% La^{3+}-TiO$_2$

C$_t$/C$_0$

Experimental time (min)

FIG. 5

FIG. 6

FIG. 7

FIG. 8

FIG.9